Self-consistent analysis of thermal far-field blooming of broad-area laser diodes

Joachim Piprek

Optical and Quantum Electronics

ISSN 0306-8919
Volume 45
Number 7

Opt Quant Electron (2013) 45:581-588
DOI 10.1007/s11082-012-9640-6

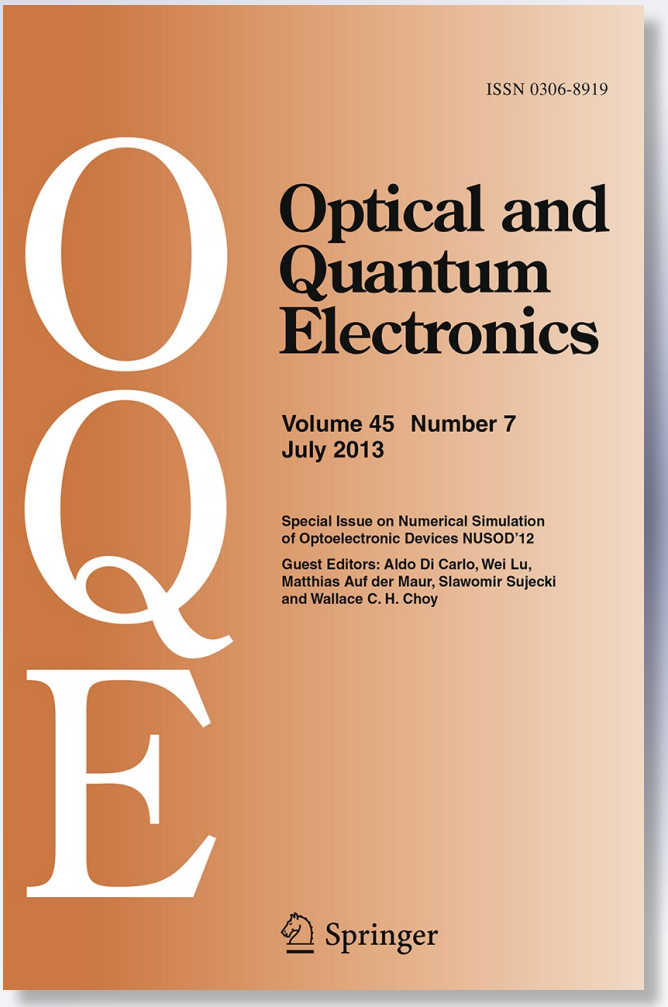

Springer

Opt Quant Electron (2013) 45:581–588
DOI 10.1007/s11082-012-9640-6

Self-consistent analysis of thermal far-field blooming of broad-area laser diodes

Joachim Piprek

Received: 28 September 2012 / Accepted: 17 November 2012 / Published online: 30 November 2012

Abstract High-power broad-area laser diodes often suffer from a widening of the lateral (slow axis) far-field with increasing current, called thermal blooming, which is mainly caused by the non-uniform self-heating of the laser and has been studied for several decades. This paper presents the first self-consistent electro-thermal-optical simulation and analysis of such thermal blooming. Using a real InGaAs/GaAs broad-area laser as an example, a 900 A/cm^2 higher current density is shown to lead to only 0.5 K stronger lateral temperature drop inside the ridge waveguide but to a one degree wider slow axis far field. Small non-thermal blooming is also observed.

Keywords High-power broad-area laser diode · Thermal blooming · Slow axis far field · Self-heating · Thermal lens · Lateral laser modes

1 Introduction

High-power broad-area laser diodes often suffer from a widening of the lateral (slow axis) far-field with increasing current (see, e.g., Crump et al. 2012). This effect is also referred to as thermal blooming, since self-heating is considered the main cause. The non-uniform temperature profile inside the waveguide leads to a lateral refractive index profile that enhances the index guiding of lateral laser modes (thermal lens). Numerical simulation is a valuable tool in investigating this sophisticated interaction of electronic, thermal, and optical processes, however, a comprehensive numerical analysis has not been published yet. Previous simulation reports use simplified models (e.g., Hadley et al. 1988), neglect the self-heating (e.g., Lang et al. 1991; Hess et al. 1995), or only combine optical and thermal models (e.g., Pomplun et al. 2012).

This paper presents the first self-consistent electro-thermal-optical simulation of the thermal blooming effect, including the non-uniform heat power distribution inside the laser as

J. Piprek (✉)
NUSOD Institute LLC, Newark, DE 19714-7204, USA
e-mail: piprek@nusod.org

well as the non-uniform carrier and gain distributions inside the quantum wells (QWs). A previously investigated GaAs-based broad-area distributed feedback (DFB) laser structure with an emission wavelength near 975 nm is used as an example (Crump et al. 2010; Schultz et al. 2010; Wenzel et al. 2011). The compressively strained double quantum well InGaAs active region is sandwiched between AlGaAs waveguide and cladding layers. The ridge-waveguide laser is mounted p-side down onto a CuW submount. The p-doped ridge is 100 μm wide and the laser cavity is 3 mm long.

2 Models and parameters

A customized version of the LASTIP laser simulation software is employed here (Crosslight Software 2012), which allows for the self-consistent combination of multi-mode wave guiding, drift-diffusion of electrons and holes, quantum well gain computation, and heat flow in the transverse plane. All relevant heat sources are considered, including Joule heat, non-radiative recombination heat, heat caused by modal absorption, as well as the Peltier/Thomson effect (Wachutka 1990). Thermal conductivity data for each layer account for alloy scattering of phonons (Nakwaski 1988). The local refractive index N(T) is calculated from the temperature distribution T(x,y) using published material parameters (Gehrsitz et al. 2000). The average (modal) thermal index change is $dN/dT = 3 \times 10^{-4}/K$. Free-carrier absorption by holes ($k_p = 12 \times 10^{-18} cm^2$) and electrons ($k_n = 4 \times 10^{-18} cm^2$) is considered as well as carrier-induced index changes in the quantum well with an anti-guiding parameter of $dN/dn = -10^{-20} cm^3$. Besides the semiconductor chip, the simulation domain also includes the p-side metal and heat spreading layers to accurately calculate the temperature profile T(x,y). The heat sink thermal conductivity is slightly varied to match the measured thermal resistance in the simulation (4.6 K/W). Transversal laser modes are calculated self-consistently from the Helmholtz equation. The modal far-fields are obtained from the Fourier transform of the modal near-field at the laser facet (Carroll et al. 1998). Further details on models and parameters are given elsewhere (Piprek 2003).

3 Simulation results

The simulated light-current and current-voltage characteristics are shown in Fig. 1a and they are in excellent agreement with measurements (Schultz et al. 2010). Figure 1b shows the calculated light-current characteristics for each of the different lateral lasing modes. The mode order corresponds to the number of modal intensity peaks. The total modal intensities add up to the lasing power given in Fig. 1a. In the following, for comparison to a previous analysis (Wenzel et al. 2011), the laser performance is evaluated at two currents, I = 3.4 A and 5.8 A, corresponding to a laser power of P = 2.7W and 5.1 W, respectively. At I = 3.4 A, nine lateral lasing modes are calculated, which is close to the eight lateral modes measured at that current (Wenzel et al. 2011). The measurement also reveals additional longitudinal modes, which are not considered in this simulation. At I = 5.8A, two more lateral lasing modes are observed, both in the measurement and in the simulation.

The lasing wavelength is controlled by the DFB grating and it changes very slowly with temperature (0.07 nm/K). The peak of the QW gain spectrum red-shifts with rising temperature at a faster rate of 0.3 nm/K. Thus, in our case, the gain peak offset from the DFB wavelength shrinks with increasing current (Fig. 2a) and a *lower* QW carrier density is

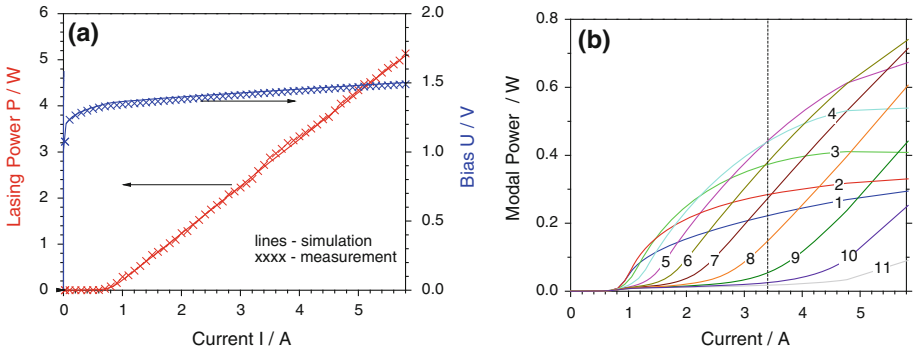

Fig. 1 **a** Comparison of simulated laser characteristics to measurements from (Schultz et al. 2010). **b** Calculated modal power versus current (parameter: mode order)

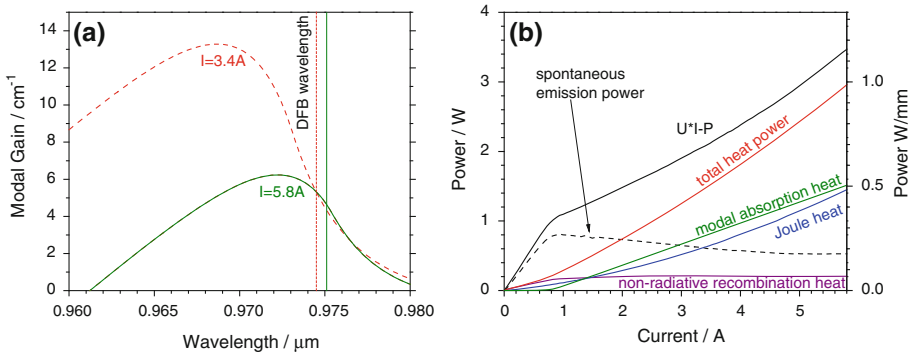

Fig. 2 **a** Modal gain spectra at two bias points, the *vertical lines* give the corresponding DFB wavelengths. **b** Power versus current for different physical mechanisms

sufficient at the *higher* current to reach the threshold gain, leading to a reduced spontaneous emission power (Fig. 2b). Figure 2b also shows the main contributions to the heat power. The total heat power is smaller than the value UI-P extracted from measurements (Fig. 1a) because the spontaneous emission is not considered a relevant heat source in this case. Simple models indicate that most of the spontaneous emission leaves the waveguide (Mukherjee and McInerney 2007) and is absorbed by the metal contacts (top and bottom) without much influence on the temperature of the active region (see further discussion in Sect. 4).

Figure 3 depicts different vertical profiles in the center of the laser (symmetry plane) at I = 5.8 A injection current: energy band diagram, refractive index, main heat sources, and light intensity. The heat generation profile from modal absorption follows the vertical shape of the laser mode. Non-radiative recombination peaks inside the quantum wells. Joule heat is mainly generated on the p-side due to the lower conductivity.

Figure 4a gives the lateral profile of the total heat generation inside the top quantum well at the two bias points. It peaks near the p-contact edge which is mainly caused by current crowding. Figure 4b shows the calculated temperature profiles. At 5.8 A, the QW temperature is about 16 K higher than the external temperature of 300 K, while the lateral temperature drop inside the ridge waveguide region ($x < 50\mu m$) is only 1 K. This lateral temperature

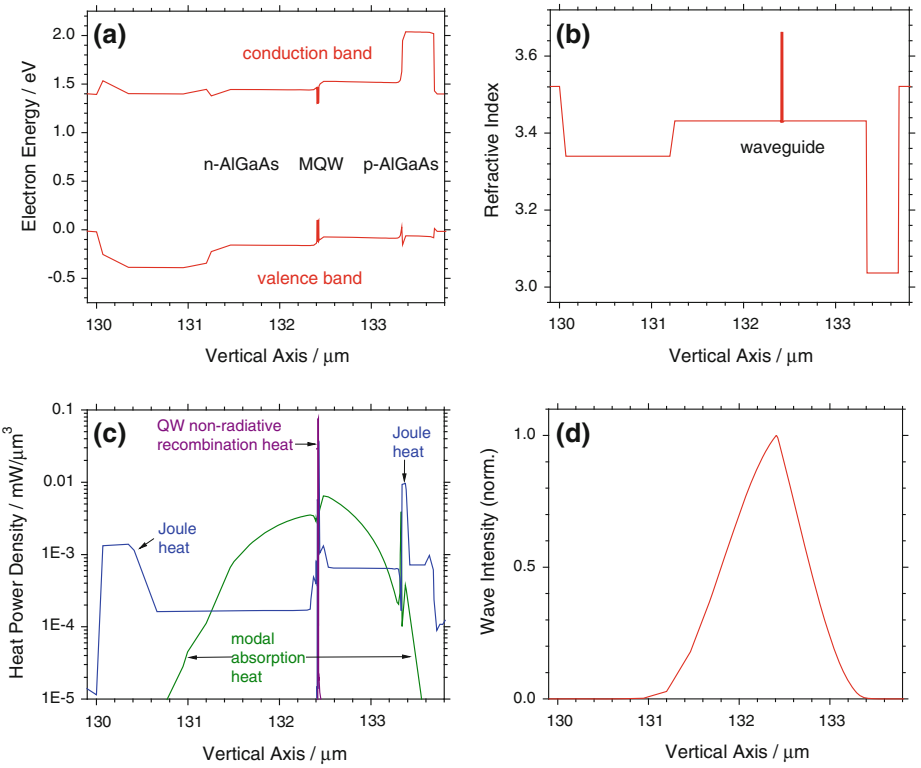

Fig. 3 Vertical profiles in the center of the laser at I = 5.8A: **a** energy band diagram, **b** refractive index, **c** main heat sources, **d** laser beam

drop increases with current, it is only 0.5 K at 3.4 A. Thus, the rising current results in stronger lateral index guiding (Fig. 4c). The lateral index difference *inside* the ridge waveguide (thermal lens) is only 0.0003 at 5.8 A and it is significantly smaller than the built-in lateral effective index step of 0.0018 at the edge of the ridge.

The QW gain profile is plotted in Fig. 4d, it turns into absorption outside the ridge region ($x > 50\mu m$) due to the drop in carrier density (Fig. 4e). As pointed out above, the QW carrier density decreases with higher current, so that the carrier-induced QW index change is also reduced (Fig. 4f). Considering the QW optical confinement factor of 0.0133, the carrier-induced effective index change is −0.0002, but it is almost constant across the ridge region, so that it does not weaken the thermal lens much. Our previous publication (Piprek 2012) employed a 2.5 times higher anti-guiding parameter dN/dn, still within the range reported in the literature (Rideout et al. 1990), which led to about double the number of lateral modes (see discussion in Sect. 4).

The lateral width of the total near field profile hardly changes with rising current (Fig. 5, LHS), which agrees very well with near field measurements (Wenzel 2012). The same figure clearly shows the thermal blooming effect, i.e., a widening of the total far field with current. While the current density rises by 900 A/cm^2, the 95 % power angle widens by one degree, from 4.6° to 5.6°. This blooming rate is in good agreement with (Wenzel et al. 2011) but below the values reported for other lasers (Chin et al. 2011). Since the total near field does not shrink, the thermal blooming is mainly attributed to the increasing number of lateral

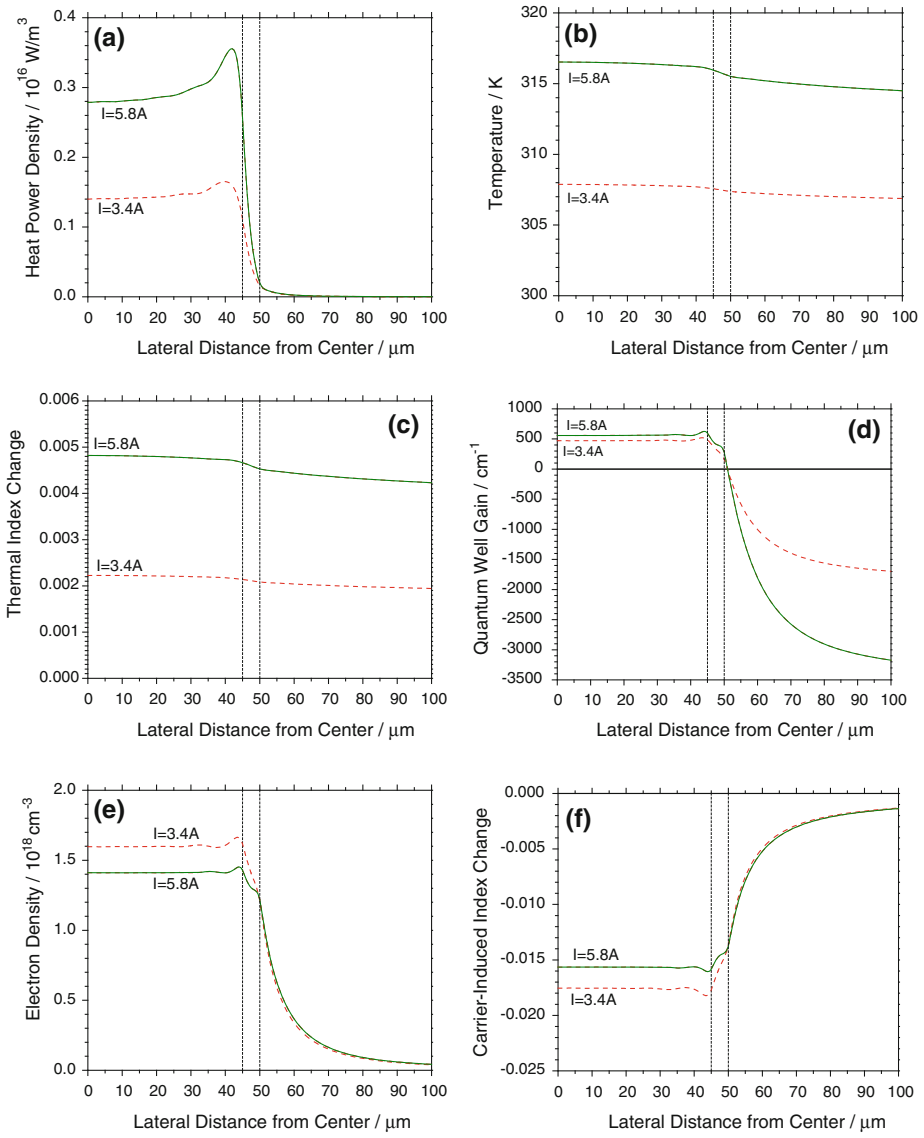

Fig. 4 Lateral profiles inside the top quantum well at two currents: **a** heat power density, **b** temperature, **c** thermal index change, **d** quantum well gain and absorption, **e** electron density, **f** carrier-induced index change. The *vertical dashed lines* mark the edges of the p-contact (x = 45μm) and of the ridge-waveguide (x = 50μm), respectively

modes (cf. Fig. 1b). Figure 5 (RHS) plots the near- and far field profiles of all lasing modes, illustrating the rising far field angle with higher mode order. As more modes participate in the lasing process, each individual near field shrinks in lateral direction and each individual far field widens slightly.

Without heating, the slow axis far field widens from 4.1° to 4.2° (95 % power, same bias points), mainly due to increasing current crowding which leads to a broader gain region supporting higher-order lateral modes.

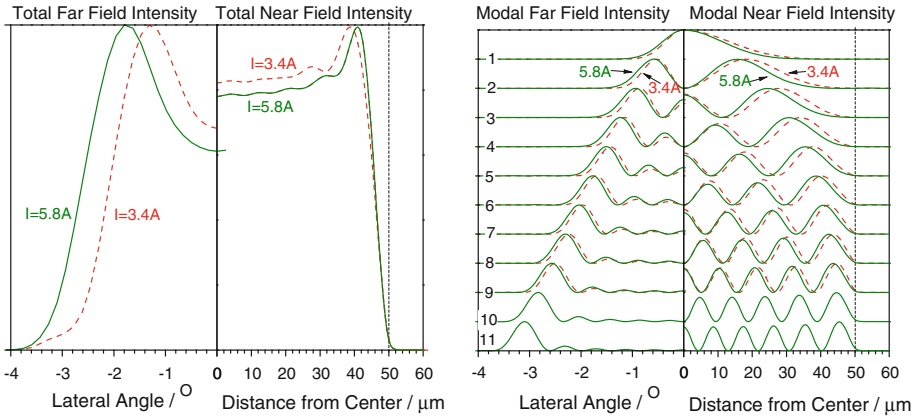

Fig. 5 Normalized intensities of the total near-fields and far-fields (LHS) and the modal near-fields and far-fields (RHS) for both bias points. The *integer numbers* give the mode order, the *vertical dashed line* marks the edge of the built-in index guide (ridge)

4 Discussion

Several experimental observations are reproduced very well by these simulations, such as the width of the total near field, the number of lateral modes and the far field blooming rate. However, the total far field angle is significantly smaller than measured (Wenzel et al. 2011), Earlier simulations produced a wider far field (Piprek 2012), but only by including lateral modes up to the 19th order, which is not supported by measurements. Possible reasons for this discrepancy are briefly discussed in the following and require future investigations.

In our model, the different lateral modes interact through the competition for the QW carrier reservoir. But in reality, modes also interfere optically, often in a random and unpredictable way, contributing to the irregular and asymmetric modal patterns observed experimentally (Wenzel et al. 2011; Crump et al. 2012). The simulation considers TE modes only, but TM emission has been measured at the fringes of the beam profiles, possibly linked to internal strain (Crump 2012). Another unexplained experimental observation with this laser is that the lateral near field width of each individual mode is much smaller than the total near field (Wenzel 2012).

Several models have been published for far-field calculations (see, e.g., Kressel and Butler 1977; Carroll et al. 1998; Piprek 2003) and due to the complexity of the thermal blooming effect, it is difficult to judge which approximation is most appropriate for the lateral far field of broad area lasers. The common Fourier transform of the near field, also employed in this paper, seems to underestimate the far field angle, which may be attributed to the neglect of the modal k-vector angle that rises with increasing mode order (Witzigmann 2012). The obliquity factor is also neglected in our model, but it is only relevant for much wider far fields (Carroll et al. 1998).

Full three-dimensional (3D) simulations are expected to provide additional insight (see, e.g., Mukherjee and McInerney 2007), since the present 2D model neglects variations in longitudinal direction as well as the influence of additional longitudinal lasing modes. An accurate account of the heat power distribution generated by the absorption of spontaneous emission is also of interest (e.g., by ray tracing); however, if this heat has any effect on the lateral far field, it would probably slightly weaken the thermal lens and the far field blooming

because the semiconductor layer exhibiting the strongest absorption is the QW region *outside* the ridge.

5 Summary

Using self-consistent two-dimensional electro-thermal-optical simulation, the physical mechanism of the thermal blooming effect in broad area lasers is investigated in detail. The widening of the far field can be attributed to a rising maximum mode order as well as to a shrinking near field of each individual mode.

Acknowledgments This work was supported by the Ferdinand Braun Institute, Berlin, Germany. The author acknowledges helpful discussions with H. Wenzel and P. Crump.

References

Carroll, J., Whiteaway, J., Plump, D.: Distributed Feedback Semiconductor Lasers. SPIE Press, Bellingham (1998)

Chin, A.K., Knapczyk, M.T., Jacob, J.H., Eppich, H., Lang, K.D., Chin, R.H.,Dogan, M.: Record CW-brightness from a single, 20% fill-factor, 1-cm laser-diode bar at 20°C. SPIE Proc. **7918**, 79180L (2011)

Crosslight Software, Inc., see www.crosslight.com (2012)

Crump, P., Schultz, C.M., Pietrzak, A., Knigge, S., Brox, O., Maaßdorf, A.,Bugge, F., Wenzel, H., Erbert, G.: 975-nm high-power broad area diode lasers optimized for narrow spectral linewidth applications. SPIE Proc. **7583**, 75830N (2010)

Crump, P., Boeldicke, S., Schultz, C.M., Ekhteraei, H., Wenzel, H., Erbert, G.: Experimental and theoretical analysis of the dominant lateral waveguiding mechanism in 975 nm high power broad area diode lasers. Sem. Sci. Technol. **27**, 045001 (2012)

Crump, P.: Ferdinand Braun Institute Berlin, Germany. Personal Communication (2012)

Gehrsitz, S., Reinhart, F.K., Gourgon, C., Herres, N., Vonlanthen, A., Sigga, H.: The refractive index of AlxGa1ÀxAs below the band gap: Accurate determination and empirical modeling. J. Appl. Phys. **87**, 7825–7837 (2000)

Hadley, G.R., Hohimer, J.P., Owyoung, A.: Comprehensive modeling of diode arrays and broad-area devices with applications to lateral index tailoring. IEEE J. Quant. Electr. **24**, 2138–2152 (1988)

Hess, O., Koch, S.W., Moloney, J.: Filamentation and beam propagation in broad-area semiconductor lasers. IEEE J. Quant. Electr. **31**, 35–43 (1995)

Kressel, H., Butler, J.K.: Semiconductor Lasers and Heterojunction LEDs. Academic Press, New York (1977)

Lang, R.L., Larsson, A.G., Cody, J.G.: Lateral modes of broad area semiconductor lasers: theory and experiment. IEEE J. Quant. Electr. **27**, 312–320 (1991)

Mukherjee, J., McInerney, J.G.: Electrothermal analysis of CW high-power broad-area laser diodes: a comparison between 2-D and 3-D modeling. IEEE J. Sel. Top. Quant. Electr. **13**, 1180–1187 (2007)

Nakwaski, W.: Thermal conductivity of binary, ternary, and quaternary III-V compounds. J. Appl. Phys. **64**, 159 (1988)

Piprek, J.: Semiconductor Optoelectronic Devices: Introduction to Physics and Simulation. Academic Press, San Diego (2003)

Piprek, J.: Self-consistent electro-thermal-optical simulation of thermal blooming in broad-area lasers. 12th NUSOD Conf., Proc. pp. 119–120 (2012)

Pomplun, J., Wenzel, H., Burger, S., Zschiedricha, L., Rozova, M., Schmidt, F., Crump, P., Ekhteraei, H., Schultz, C.M., Erbert, G.: Thermo-optical simulation of high-power diode lasers. Proc. SPIE 8255 (2012)

Rideout, W., Yu, B., LaCourse, J., York, P.K., Beernink, K.J., Coleman, J.J.: Measurement of the carrier dependence of differential gain, refractive index, and linewidth enhancement factor in strained-layer quantum well lasers. Appl. Phys. Lett. **56**, 706–708 (1990)

Schultz, C.M., Crump, P., Wenzel, H., Brox, O., Maaßdorf, A., Erbert, G., Traenkle, G.: 11W broad area 976 nm DFB lasers with 58% power conversion efficiency. Electron. Lett. **46**, 580 (2010)

Wachutka, G.K.: Rigorous thermodynamic treatment of heat generation and conduction in semiconductor device modeling. IEEE Trans. Comput. Aided Des. **9**, 1141–1149 (1990)

Wenzel, H., Crump, P., Ekhteraei, H., Schultz, C., Pomplun, J., Burger, S., Zschiedrich, L., Schmidt, F., Erbert, G.: Theoretical and experimental analysis of the lateral modes of high-power broad-area lasers. 11th NUSOD Conf., Presentation WA2 (2011)
Wenzel, H.: Ferdinand Braun Institute Berlin, Germany. Personal Communication (2012)
Witzigmann, B.: University of Kassel, Germany. Personal Communication (2012)